Pressure-induced amorphization of cubic ZrW_2O_8 studied *in situ* and *ex situ* by synchrotron x-ray diffraction and absorption

Tamas Varga, Angus P. Wilkinson, and Andrew C. Jupe
School of Chemistry and Biochemistry, Georgia Institute of Technology, Atlanta, Georgia 30332-0400, USA

Cora Lind
Department of Chemistry, The University of Toledo, Toledo, Ohio 43606-3390, USA

William A. Bassett
Geological Sciences, Department of Earth & Atmospheric Sciences, Snee Hall, Cornell University, Ithaca, New York 14853-1504, USA

Chang-Sheng Zha
CHESS, Wilson Lab, Cornell University, Ithaca, New York 14853, USA
(Received 27 February 2005; published 27 July 2005; corrected 27 December 2006)

The behavior of cubic ZrW_2O_8 on compression in a DAC to 7.6 GPa was examined *in situ* by a combination of synchrotron x-ray diffraction and x-ray absorption spectroscopy (XAS). These data were compared with x-ray absorption measurements on an amorphous sample of ZrW_2O_8 recovered from 7.5 GPa in a multianvil apparatus. The *in situ* diffraction data show the complete formation of orthorhombic ZrW_2O_8 at low pressure ($<$0.5 GPa), and amorphization onset at $>$2.4 GPa with completion at $<$7.6 GPa. The corresponding *in situ* XAS data suggest a continuous evolution of the local tungsten coordination environment on compression after forming the orthorhombic phase, with the average W—O bond length increasing, indicating an increase in the average coordination number, and the W L_I pre-edge peak decreasing in magnitude, indicating a movement toward tungsten coordination that is closer to centrosymmetric These observations are inconsistent with a model for the amorphization that simply involves a loss of orientational/positional order among existing coordination polyhedra. The XANES data for the amorphous sample recovered from the multianvil apparatus are unlike any of the XANES seen in the *in situ* measurements, suggesting that the local structure in the glassy material relaxes on decompression. The XANES for the recovered sample are very similar to those for ammonium paratungstate, a material that contains tungsten in a variety of heavily distorted octahedral environments.

DOI: 10.1103/PhysRevB.72.024117 PACS number(s): 61.50.Ks, 61.43.−j, 62.50.+p, 61.10.Nz

I. INTRODUCTION

Since the amorphization of hexagonal ice was discovered under compression,[1] pressure-induced amorphization (PIA) has been observed for many different materials.[2–11] The phenomenon is not uncommon for framework structures, and it has been observed at unusually low pressures in several negative thermal expansion (NTE) materials.[11–15] A possible theoretical link between NTE and PIA has been suggested by some authors.[16]

Negative thermal expansion materials have received considerable attention during the last decade,[17–20] driven by a combination of scientific curiosity and technological interest, as they are of potential value in composites with tailored thermal expansion. The relatively low-density and highly flexible framework structures found for many NTE materials combined with the necessary presence of lattice modes that become softer on volume reduction[21–27] predisposes them to a rich behavior at high pressures. Pressure-induced crystalline to crystalline phase transitions have been reported for cubic ZrW_2O_8,[24,25,28–31] cubic HfW_2O_8,[26,32] cubic $ZrMo_2O_8$,[12,13] cubic $HfMo_2O_8$,[13] ZrV_2O_7,[33] $Sc_2W_3O_{12}$,[34] $Sc_2Mo_3O_{12}$[35] and $Al_2W_3O_{12}$[36,37] as well as PIA at low pressures in $ZrMo_2O_8$,[12,13] ZrW_2O_8,[14] $Sc_2W_3O_{12}$,[15] $Sc_2Mo_3O_{12}$[38] and $Lu_2W_3O_{12}$.[11] Typically, the volume thermal expansion coefficient of the high-pressure phase is significantly larger (more positive) than that of the original material. For ZrW_2O_8, NTE is not totally eliminated on transforming to an orthorhombic phase,[28,29] but for materials with the orthorhombic $Sc_2W_3O_{12}$ structure NTE is likely to be lost completely, as the monoclinic structure that is formed on compression[34–36] is known to show positive thermal expansion for compositions that adopt this structure at ambient pressure.[39–41] This increase in expansion coefficient on transformation is detrimental to some possible applications, as composites containing NTE materials may be subject to high pressures during processing.[42–44]

Cubic ZrW_2O_8 has been the subject of many studies, as it displays isotropic NTE over a very wide temperature range.[45,46] Its structure,[45,47] thermal expansion mechanism[46,48–53] and high-pressure behavior have been examined.[14,21,22,24,25,28–31,54] Work on controlled thermal expansion composites for use in precision optical devices has also been conducted.[55,56] The framework consists of corner-sharing ZrO_6 octahedra and WO_4 tetrahedra, with all of the oxygen of the ZrO_6 octahedra bridging to tungsten, but one oxygen in each tetrahedron in a terminal position, giving rise to considerable structural flexibility.[47] This flexibility plays

an important role in the unusual properties of cubic ZrW_2O_8.[45,46] There is an order-disorder phase transition at around 430 K going from space group $P2_13$ to $Pa\bar{3}$, leading to an increase in the thermal expansion coefficient at this temperature.[45,46] The material displays a linear coefficient of thermal expansion (CTE) of -8.8×10^{-6} K^{-1} below the temperature of the phase transition (0.3–430 K range) and -4.9×10^{-6} K^{-1} above the phase transition (430–690 K), resulting in an average CTE of -8.7×10^{-6} K^{-1} over the range of 0.3–690 K.[45,46] From a local structure perspective, the negative thermal expansion is often viewed as originating in the transverse thermal vibrations of bridging oxygen atoms,[46] although an alternative explanation with almost rigid Zr—O—W links has been proposed.[57,58] From the perspective of lattice dynamics, the NTE apparently primarily originates from low-energy vibrations, in which the WO_4 and ZrO_6 polyhedra are essentially rigid.[22,53,59–62] In a high-pressure inelastic neutron diffraction study of cubic ZrW_2O_8 the negative thermal expansion was attributed to modes below 8 meV that showed significant softening on compression and hence had large negative Grüneisen parameters.[22] However, some high-pressure Raman spectroscopic studies have indicated that in addition to the low-frequency rigid unit modes, several other modes also have negative Grüneisen parameters and hence contribute to the NTE.[24,25]

High-pressure diffraction studies of cubic ZrW_2O_8 have uncovered a transition to orthorhombic γ-ZrW_2O_8 starting at ~0.2 GPa,[28,29] followed by progressive PIA in the range 1.5 to 3.5 GPa,[14,24,25] Glassy phases resulting from pressure-induced amorphization are often considered to be metastable intermediates between a crystalline starting material and one or more crystalline products. The glass forms as a result of kinetic hindrance to the equilibrium transformation. Numerous structural mechanisms have been proposed for pressure-induced amorphization, some of which are related and can be simultaneously in operation.[4,6,7,16,63,64] Based on *ex situ* high-pressure x-ray diffraction and Raman spectroscopic studies on cubic ZrW_2O_8, it has been proposed that above 1.5 GPa, tilting and deformation of the ZrO_6 and WO_4 polyhedra leads to the loss of crystallinity as the material becomes denser.[14,65] *In situ* high-pressure neutron diffraction experiments were interpreted in terms of tungsten with 4, 4+1, and 4+2 coordination in the orthorhombic (γ) phase.[28] On the basis of high-pressure simulations, it has been argued that these extra tungsten-oxygen "short" contacts do not play a big role in bonding and that the structure of the orthorhombic (γ) phase should really be viewed as consisting of WO_4 tetrahedra with some oxygens that are close to the tetrahedra and impede large-amplitude vibrations involving their motion.[62] Additionally, it was argued that at high pressure, major coordination changes involving the zirconium were more likely than those involving tungsten.[62] Raman studies of ZrW_2O_8 were interpreted as indicating amorphization at 2.2 GPa due to a kinetically hindered pressure-induced decomposition into its constituent oxides.[24,25] The preparation of a new ZrW_2O_8 polymorph with a cation-disordered α-U_3O_8-type structure by heating a pressure-amorphized sample under pressure suggested that the amorphization process may involve an increase in coordination number.[54] The Zr and W cations in this structure display 6+1 coordination,[54] indicating that the tetrahedral coordination of tungsten in cubic ZrW_2O_8 and the predominantly 4+1 coordination of tungsten in orthorhombic ZrW_2O_8[28] are unstable at high pressure.

In order to directly probe the mechanism of amorphization in ZrW_2O_8, *in situ* high-pressure measurements examining local structure are desirable. An *in situ* experiment avoids structural relaxation on pressure release, a phenomenon that is well known in high-pressure studies of glasses,[66,67] and facilitates the study of changes in the structure during compression and decompression. The local structure of glasses can be probed directly by total scattering, x-ray absorption spectroscopy (XAS) and other spectroscopic probes such as NMR, but the use of these techniques at high pressure is nontrivial. X-ray total scattering data recorded from samples in diamond anvil cells (DACs) has been employed to study local structure under pressure,[68,69] but the methodology is still under development.[69] High-pressure XAS (EXAFS and XANES)[70,71] is somewhat better developed, but still very challenging. The main difficulty associated with high-pressure XAS is diffraction from diamonds if a DAC is employed. Diffraction can make a strong contribution to the measured attenuation at certain x-ray energies and orientations of the diamonds,[72–74] leading to potentially quite broad peaks (glitches) in the spectra. There are several methods for avoiding these glitches. Energy dispersive EXAFS facilitates the rapid screening of cell orientations for one that has no or very few glitches.[75,76] The use of polycrystalline B_4C for both anvils eliminates the problem at the expense of complicating pressure calibration as the optically opaque anvils preclude the use of the ruby fluorescence method;[71] some workers have opted to use one diamond and one polycrystalline anvil to get around this issue.[71,77] Data can be taken using a DAC by employing a low atomic number gasket and recording spectra through the gasket rather than the diamonds.[78,79] A multianvil apparatus can be employed.[80] If transmission data is recorded through the diamonds of a DAC, the glitches can, in principle, be eliminated by measuring spectra at several different orientations of the cell, so that the glitches appear at different energies, and then producing a composite spectrum.[70]

Here we report an *in situ* high-pressure, combined XAS and diffraction study of cubic ZrW_2O_8. Diffraction probes the loss of long-range order on compression and XAS probes the corresponding changes in local environment. Changes in the local coordination environment provide insight into the mechanism by which the material becomes amorphous under pressure. Single crystal diamond anvils were used for these studies as the diffraction background from polycrystalline anvils would have been unacceptable. XAS data on an amorphous ZrW_2O_8 sample recovered from high pressure are also reported.

II. EXPERIMENTAL

A. Syntheses

1. Cubic ZrW_2O_8

A stoichiometric amount of $ZrO(NO_3)_2\cdot xH_2O$ (Aldrich, Milwaukee, WI) was thoroughly mixed and ground with

2 wt% excess of H_2WO_4 (Strem Chemicals, Newburyport, MA). The powder was heated at 1150 °C for 5, 24, and 36 h periods with intermittent ice-water quenching, drying (at 130 °C) and regrinding steps.

2. Amorphous ZrW_2O_8

Cubic ZrW_2O_8 was compressed using a Walker-type high-pressure multianvil press at the Mineral Physics Institute, SUNY Stony Brook, NY. The pressure cell consisted of a platinum sample capsule in a 14 mm magnesia octahedron surrounded by eight one-inch tungsten carbide cubes, all truncated on the corner facing the magnesia. Pyrophyllite and teflon gaskets as well as balsa spacers were used between the cubes. ~140 mg of cubic ZrW_2O_8 was placed into the Pt capsule and the sample was exposed to a pressure of about 7.5 GPa at room temperature for 2 h prior to slow decompression.

3. Ba_2NiWO_6

$BaCO_3$, $NiCO_3$, and WO_3 were thoroughly mixed and ground. The mixture was heated at 1100 °C for 20 h and, after regrinding, heated at 1400 °C for an additional 2 h.

4. $Sc_2W_3O_{12}$

Sc_2O_3 and WO_3 were mixed, ground, and heated together at 1000 °C for 5 h, then, after regrinding, heated at 1200 °C for 12 h.

The reference compounds $Na_2WO_4 \cdot 2H_2O$, $(NH_4)_{10}W_{12}O_{41} \cdot 5H_2O$ (Alfa Aesar, Ward Hill, MA) and WO_3 (Aldrich, Milwaukee, WI) were used as received.

B. Diamond anvil cell

A so-called "hydrothermal diamond anvil cell" (HDAC)[81,82] was used with NaCl as a pressure calibrant, sample diluent, and pressure transmitting medium. ~1.7 mm thick diamonds with 500 μm culet faces were employed along with a 125 μm thick rhenium gasket that had a 300 μm sample hole. The gasket was preindented to a pressure of about 10 GPa. The downstream cone opening of the cell was ~44 deg. The sample was uniformly mixed and ground with NaCl and packed into the HDAC with a ratio (ZrW_2O_8:NaCl) of ~1:4. This ratio was chosen to give an approximate μt for the sample (excluding the diamonds) of 2.

C. Diffraction data collection

Diffraction data were collected at room temperature and up to 7.6 GPa pressure using the B-2 line of the Cornell High Energy Synchrotron Source (CHESS), Wilson Lab, Cornell University, Ithaca, NY. An x-ray energy of 17.968 keV was selected using a Ge(111) double-crystal monochromator. The beam was collimated to ~130 μm diameter, and centered onto the sample cavity of the DAC. Diffraction patterns were recorded on image plates using ~5 min exposures. The sample-to-plate distance was calibrated using diffraction from NaCl in the initially closed HDAC. As the initial pressure was slightly above ambient, there are minor pressure calibration errors (see Sec. III). The image plates were read using a BAS 2000 scanner and integrated to give intensity versus 2θ values using the SIMPA software.[83] The integrated patterns were then processed in JADE[84] for pressure calibration and visualization purposes. The identification of orthorhombic ZrW_2O_8 was performed using the program package GSAS.[85] NaCl diffraction angles obtained by fitting in JADE were used along with the program CALIBRATION[86] for pressure determination. CALIBRATION makes use of the Birch equation of state for NaCl.[87] As the pressure was increased, diffraction data were collected at each pressure point. The resulting data are shown in Fig. 1. At selected pressures (0.0, 0.7, 2.3, 3.6, and 7.6 GPa) the experimental arrangement was adjusted so that XANES and EXAFS data could be collected.

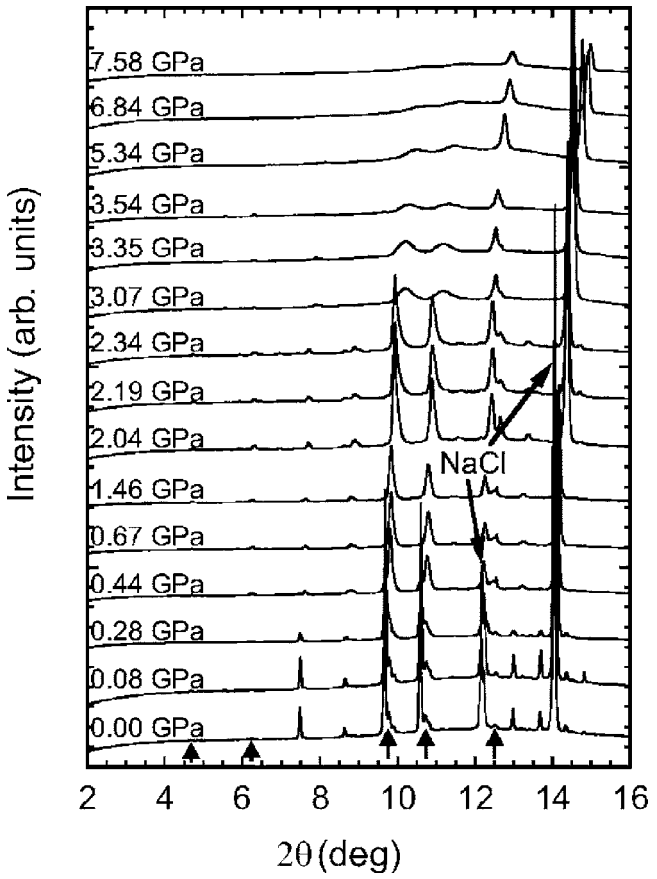

FIG. 1. Powder diffraction patterns for ZrW_2O_8 as a function of pressure. Arrows indicate the location of peaks characteristic of the orthorhombic phase. The NaCl calibrant peaks are also marked. The data were collected at 17.968 keV (λ=0.6901 Å).

D. EXAFS and XANES data collection

The XAS measurements were carried out at the same beamline (B-2 line at CHESS) in parallel with the diffraction measurements using the same double crystal monochromator and collimator. Data were collected at room temperature in the 0–7.6 GPa pressure range. The transmission XAS measurements made use of three ion chambers with the DAC between the first and second detector and a reference metal

foil between the second and third detector. The reference foil data were used to ensure that the sample spectra were on a common energy scale. Swapping between diffraction and XAS measurements involved removing the beam stop and the image plate holder from the optical bench and replacing them by the transmission and reference ion chambers, and then changing the energy from ~18 keV to that of the appropriate tungsten absorption edge.

XAS data were collected for cubic ZrW_2O_8, $Sc_2W_3O_{12}$, Ba_2NiWO_6, $Na_2WO_4 \cdot 2H_2O$, $(NH_4)_{10}W_{12}O_{41} \cdot 5H_2O$, and WO_3 at ambient pressure and temperature using samples that were diluted and ground with boron nitride and then packed into aluminum sample holders with Kapton tape windows so that the maximum value of μt was 1.5–2. EXAFS scans were performed at the W L_{III} edge (9.85–10.90 keV) and XANES data were recorded at the W L_I edge (12.025–12.200 keV) using 50% monochromator detuning for harmonic rejection. For the L_{III}-edge EXAFS, a three region scan was employed with 10 eV steps in the pre-edge region (9.85–10.19 keV), 0.5 eV steps in the near-edge region (10.19–10.22 keV) and 2 eV steps in the post-edge region (10.22–10.90 keV). XANES data at the L_I edge were recorded using three region scans with 5 eV steps in the pre-edge region (12.025–12.060 keV), 1.0 eV steps in the near-edge region (12.060–12.150 keV) and 2 eV steps in the post-edge region (12.150–12.200 keV). Data at each point were recorded until a preset number of monitor counts was achieved, taking approximately 4 s per point, and three scans were performed for each sample.

XAS data for the ZrW_2O_8 sample in the DAC were collected at several different orientations of the DAC so that the glitches due to diffraction from the diamonds occurred at different energies. The DAC was mounted on a "V" block above a rotation stage so that it could be reoriented around a vertical, ω, axis. As the DAC casing was smooth and cylindrical, the DAC body could be manually rotated in the V block about the cylinders axis providing for a χ-type rotation (ω and χ are used here in the sense of a Eulerian cradle diffractometer). 8 to 10 different cell orientations were used at each pressure, with one scan in each orientation. While widely different values of χ were used ($\sim \pm 30°$), ω was only varied by $\sim \pm 1.5°$ among these scans.

E. Processing of XAS data recorded at ambient conditions

Data processing was performed using the program ATHENA.[88,89] At least three energy scans were averaged for each sample. All data were put on a common energy scale using the reference foil absorption spectra.

F. Processing of XAS data from the DAC

Glitches arising from diamond diffraction severely contaminated the recorded XAS at each orientation of the DAC. In general, this problem is a function of the edge energy that is being examined and the energy range over which data is required. The number of glitches in a given energy range increases approximately with the square of the edge energy and for tungsten, in practice, it was not possible to find a single diamond cell orientation that did not give glitches in the energy range of a useful XANES or EXAFS energy scan. This problem is compounded by the presence of two diamonds in the beam with different crystallographic orientations and by the strains that are introduced into the diamonds as the cell pressure increases. The strain gradients that arise from loading the diamonds effectively increase their mosaic spread and broaden the range or energies/orientations over which they give rise to glitches. Rather than attempting to obtain glitch-free data directly, we have instead carried out multiple data collections with different orientations of the DAC with respect to the incident beam and then processed these data to obtain composite spectra that are largely free from glitches at low pressure.

Initially, in each raw energy scan, regions containing glitches were selected by eye and the glitch replaced by an interpolated straight line. The locations of these regions were tracked so that they could be excluded from the final summation. We ensured that each scan was on a common energy scale by determining the apparent absorption edge energy for the scan using the simultaneously collected reference foil data. This procedure made use of the program ATHENA.[88] ATHENA was then used to background subtract and normalize the individual energy scans giving $\chi(k)$ for each scan. A composite $\chi(k)$ was created by summing the available individual energy scans (excluding the interpolated regions) and dividing by the number of contributing scans at each point. Typically, two to four scans at different orientations contributed to each point in the composite $\chi(k)$. However, for the higher-pressure data, where strain in the diamonds led to a worse glitch problem, it was not possible to construct complete composite spectra without glitches. The composite spectra are shown in Fig. 2.

G. Analysis of the XANES and EXAFS data

The raw XANES spectra were background subtracted, normalized, and plotted for comparison. Figure 3 shows spectra from a series of model compounds along with those for cubic ZrW_2O_8 and amorphous ZrW_2O_8 that had been recovered from ~7.5 GPa in a multianvil press. In Fig. 4, XANES spectra recorded in the DAC at different pressures are compared to one another.

All EXAFS data fits were performed using the program ARTEMIS.[88,89]As the data obtained in the DAC was of low quality due to a combination of a poor signal to noise ratio and the glitch problem, a very simple model was adopted as a baseline for the analysis of all the EXAFS data. In EXAFS analyses there are often problems with correlations between estimated pathlengths and E_0, and Debye–Waller factors and the amplitude reduction factor. We chose to estimate E_0 and S_0 (the amplitude reduction factor) using the data for $Na_2WO_4 \cdot 2H_2O$ and then use these values in all of our subsequent fits. The first shell for $Na_2WO_4 \cdot 2H_2O$ was fit, in both q space (Fourier filtered k space) and R space, using the crystallographic model for this compound with the Debye-Waller factor for all paths fixed at 0.002 $Å^2$, based on an inspection of literature values for W—O bonds, and E_0, S_0, and Δr (the deviation of bond lengths from their initial val-

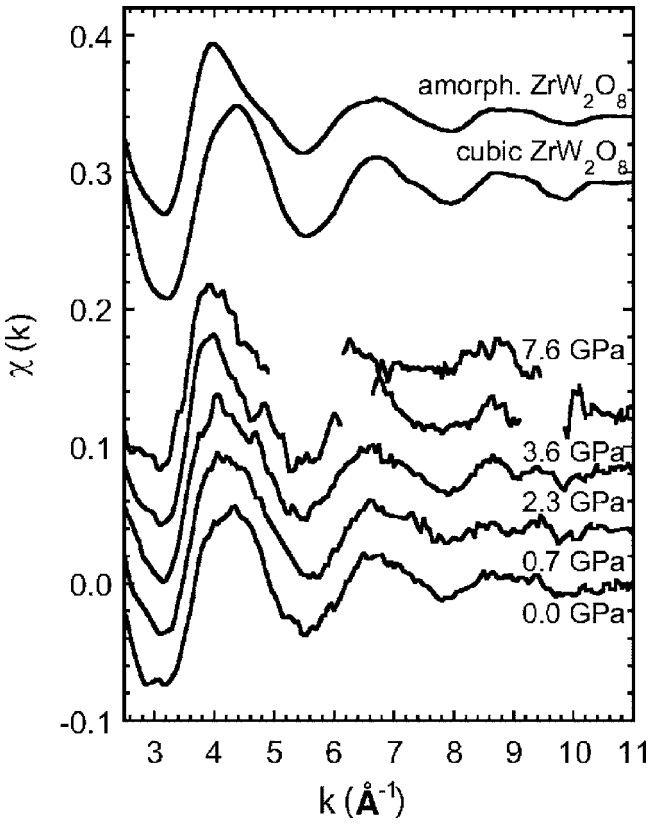

FIG. 2. W L_{III} $\chi(k)$ for ZrW_2O_8 as a function of pressure along with those for cubic (outside the pressure cell) and preamorphized ZrW_2O_8 samples. The missing sections of the 3.6 and 7.6 GPa data arise because we were unable to eliminate the glitches from these regions using the available data.

ues) as variable parameters. The first shell in the ambient pressure data for all the model compounds, amorphous ZrW_2O_8, and the DAC data was then fit in both q and R space using fixed values of E_0 and S_0. The baseline model for all of the first shell data was a single W—O scattering path with Δr and σ^2, a Debye-Waller factor, as variables. Fits were once again performed in both R and q space. Additionally, a model for the amorphous ZrW_2O_8 based on the known crystal structure of orthorhombic ZrW_2O_8 (Ref. 28) was used to fit the *ex situ* data for this compound and the DAC data. All the fits were performed using the same q- (2.5–11 Å^{-1}) and R ranges (0.85–1.80 Å). The tabulated results are available as supplementary material.[108]

III. RESULTS AND DISCUSSION

A. High-pressure diffraction

The diffraction data from our DAC measurements are shown in Fig. 1. The closed cell diffraction pattern, marked as 0.00 GPa, shows the presence of a small quantity of orthorhombic ZrW_2O_8 (~9% from the Bragg peak areas), along with the expected cubic ZrW_2O_8 and NaCl, indicating that the pressure in some parts of the sample must be slightly above ambient. As our calibration procedure assumed that this closed cell data was at ambient pressure, all of our subsequent pressure estimates are likely to be slightly too low.

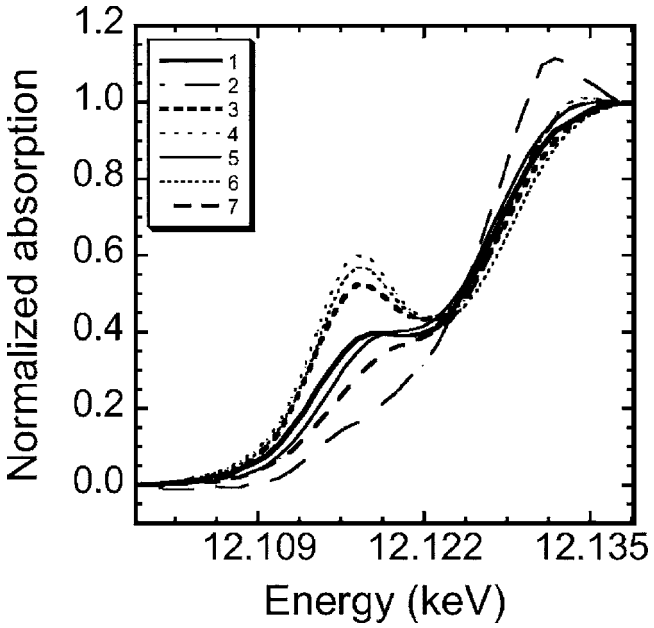

FIG. 3. W L_I XANES for a series of reference compounds with different tungsten coordination environments: (1) amorphous ZrW_2O_8 recovered from 7.5 GPa, (2) Ba_2NiWO_6—octahedral, (3) cubic ZrW_2O_8—tetrahedral, (4) $Na_2WO_4 \cdot 2H_2O$—tetrahedral, (5) $(NH_4)_{10}W_{12}O_{41} \cdot 5H_2O$—heavily distorted 6 coordinate, (6) $Sc_2W_3O_{12}$—tetrahedral, and (7) WO_3—distorted octahedral.

The transformation of the cubic phase to the orthorhombic phase appears to be well advanced at 0.28 GPa and complete by 0.44 GPa. There is substantial line broadening in the diffraction pattern of the ZrW_2O_8 at pressures higher than 3 GPa, and by 7.6 GPa there is no evidence of any Bragg peaks from the ZrW_2O_8, suggesting the formation of a glassy product. Our data indicate the onset of amorphization above ~2.5 GPa, with completion of the process at >5 GPa. This

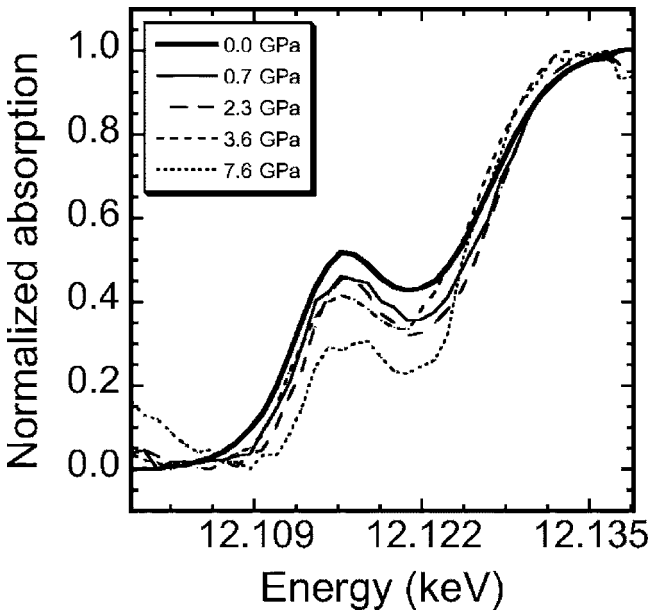

FIG. 4. W L_I XANES for ZrW_2O_8 under pressure in a DAC.

TABLE I. The first-shell W—O average bond lengths obtained from the EXAFS data for a series of reference compounds, with different W coordination, and compressed ZrW_2O_8 at different pressures. The fits were carried out in Fourier-filtered k space using only one scattering path (k range: 2.5–11 $Å^{-1}$, R range: 0.85–1.80 Å).

		Aver. W—O bond length (Å)	
	Sample/Pressure	4 coord.	6 coord.
Ex situ (outside DAC)	$Sc_2W_3O_{12}$ (tetrahedral) (Ref. 105)	1.760(4)	1.765(14)
	Cubic ZrW_2O_8 (tetrahedral) (Ref. 45)	1.765(8)	1.769(19)
	$Na_2WO_4 \cdot 2H_2O$ (tetrahedral) (Ref. 106)	1.767(4)	1.771(14)
	Amorphous ZrW_2O_8	1.803(18)	1.815(29)
	WO_3 (distort. octahedr.) (Ref. 107)	1.822(24)	1.838(34)
	$(NH_4)_{10}W_{12}O_{41} \cdot 5H_2O$ (irregular 6-coord.) (Ref. 99)	1.832(15)	1.839(23)
	Ba_2NiWO_6 (octahedral) (Ref. 104)	1.871(10)	1.875(3)
In situ (in DAC)	ZrW_2O_8/0.0 GPa	1.776(9)	1.783(21)
	ZrW_2O_8/0.7 GPa	1.775(11)	1.783(21)
	ZrW_2O_8/2.3 GPa	1.793(14)	1.802(26)
	ZrW_2O_8/3.6 GPa	1.810(14)	1.820(25)
	ZrW_2O_8/7.6 GPa	1.861(27)	1.871(37)

onset pressure is higher than that reported by some other workers (1.5 GPa),[14] but consistent with previous Raman studies.[24,25] This discrepancy may be related to differing stress states for the samples.[90–94]

B. *Ex situ* XANES

XANES is sensitive to both the oxidation state and site symmetry of an absorbing atom; see, for example, the early work of Wong.[95] For 3*d* metals, sensitivity to site symmetry is typically achieved by examining the behavior of a pre-edge feature in the *K*-edge spectra that arises primarily from a 1*s* to *nd* transition that is dipole forbidden in a centrosymmetric coordination environment, but is observed in non-centrosymmetric environments. If only *L*-edge spectra can be recorded, similar sensitivity can be obtained at the L_I-edge (2*s* to *nd* transitions). There have been several studies using W L_I XANES to probe absorber oxidation state and site symmetry.[96–98]

In Fig. 3, we show W L_I-XANES spectra for a series of model compounds containing tungsten in different coordination environments along with a XANES spectrum for the amorphous ZrW_2O_8 recovered from 7.5 GPa in a Walker press (see Table I for the coordination geometries). The XANES from cubic ZrW_2O_8, $Na_2WO_4 \cdot 2H_2O$, and $Sc_2W_3O_{12}$ are very similar to one another, showing a pronounced pre-edge peak consistent with a coordination environment that is far from centrosymmetric. In all of these compounds, the tungsten is tetrahedrally coordinated. This pre-edge feature is much weaker in the XANES from ammonium paratungstate, a compound that contains tungsten in heavily distorted octahedral coordination environments (W—O ranges from ~1.75–2.25 Å for many of the tungsten sites).[99] In ambient pressure WO_3, the pre-edge feature is weaker still, indicative of a more regular coordination, although there is still considerable distortion in the pseudo-octahedral tungsten coordination environment.[100] The data for Ba_2NiWO_6 has almost no pre-edge feature, as expected for a perovskite with regular octahedral tungsten coordination.[101] The pre-edge feature for the amorphous ZrW_2O_8 is very similar to that observed for the paratungstate. This indicates that compression has destroyed the original tetrahedral coordination of the tungsten, ruling out a simple polyhedral tilting model for the amorphization. It also indicates that the final product does not predominantly contain tungsten in an octahedral or slightly distorted octahedral coordination environment. However, it may contain tungsten in heavily distorted octahedral or perhaps five-coordinate environments. The loss of predominantly tetrahedral coordination is expected on compression as orthorhombic ZrW_2O_8 is known to form at 0.2–0.4 GPa, and this phase contains a mixture of 4-, 4+1- and 4+2-coordinate tungsten, with predominantly 4+1 coordination.[28] The XANES data are inconsistent with a simple-minded view of a kinetically frustrated pressure-induced demixing driving the amorphization, as the pre-edge in the amorphous material is more pronounced than that of ambient pressure WO_3. However, tungsten in WO_3 is known to undergo significant coordination changes on compression[100] and at ambient temperature a kinetically frustrated decomposition could not proceed very far, perhaps, leading to more distorted coordination than that in ambient pressure WO_3. ZrW_2O_8 has been reported to transform on heating under pressure to a dense phase with a structure related to that of α-U_3O_8.[54] The highly irregular 6+1 coordination reported for the metals in this phase may be compatible with the XANES data.

C. *In situ* XANES

XANES data for ZrW_2O_8 as it is compressed in the DAC are shown in Fig. 4. In general, the intensity of the pre-edge feature drops as the pressure is increased. There is an initial drop in the size of this feature on going from ambient pressure to 0.7 GPa and a further decrease above 2.3 GPa. The diffraction patterns for the sample at 0.7 and 2.3 GPa both indicate the presence of single phase orthorhombic ZrW_2O_8, so the initial change in the pre-edge feature is due to the transformation of cubic ZrW_2O_8, containing only tetrahedral tungsten (1+3 coordination), to orthorhombic ZrW_2O_8, with primarily 4+1 coordination for the tungsten. At 3.6 GPa, the diffraction data still show very broad weak scattering maxima in the positions expected for the orthorhombic phase, suggesting incomplete disordering or considerable strain broadening, but as the FWHM for NaCl(200) at this pressure is similar to that at lower pressures, the peak broadening of the ZrW_2O_8 is probably due to disordering rather than just strain broadening. The pre-edge feature in the

XANES at 3.6 GPa is only slightly less pronounced than that at 2.3 GPa, indicating that the disordering is not associated with large changes in coordination symmetry. Further compression to 7.6 GPa leads to a dramatic decrease in the magnitude of the pre-edge feature, suggesting a move toward a coordination environment that is much closer to centrosymmetric. The 7.6 GPa XANES are not consistent with distorted six-fold coordination, such as that seen in the ambient pressure ammonium paratungstate or WO_3 (see Fig. 3), but they could indicate residual 4+1 coordination in a matrix that contains almost centrosymmetric tungsten, or possibly a residual diamond diffraction glitch superimposed on XANES from almost centrosymmetric tungsten. The diffraction data recorded at this pressure show that the sample is glasslike.

It is notable that none of the XANES spectra recorded in the DAC under pressure resemble the XANES for the amorphous sample recovered from the Walker cell (shown in Fig. 3). The DAC data always show a pre-edge peak that is well separated from the edge, whereas the *ex situ* data show a pre-edge feature that is starting to merge into the edge. The differences between the *in situ* and *ex situ* measurements probably arise from structural relaxation on decompression of the material that was prepared in a multianvil device, but the different stress states in the DAC and multianvil device may play a role. The sample in the DAC may have been closer to hydrostatic than in the multianvil apparatus due to the presence of large amounts of relatively soft NaCl mixed in with the DAC sample. The ambient pressure bulk modulus, B_0, for NaCl is ~25 GPa[87,102] and for orthorhombic ZrW_2O_8 it is ~65 GPa.[30]

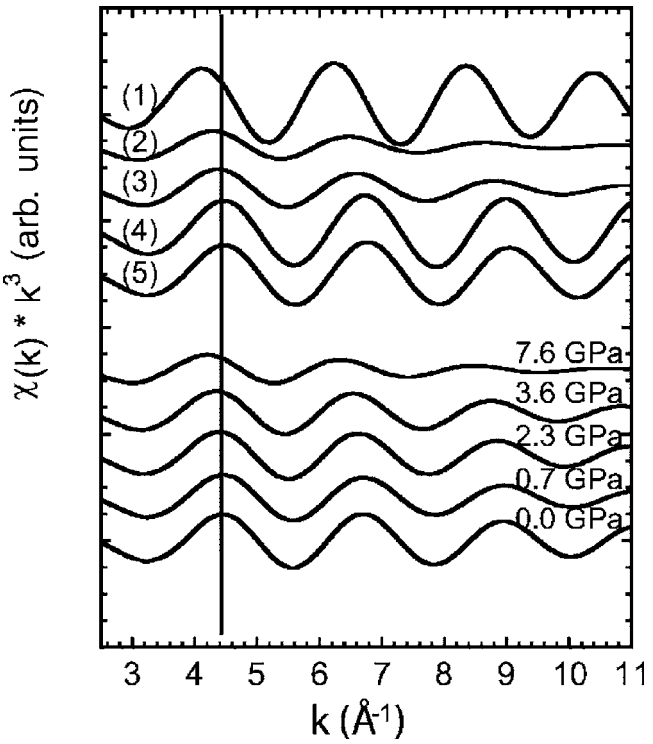

FIG. 5. A comparison of Fourier-filtered first-shell EXAFS data at ambient pressure from (1) Ba_2NiWO_6, (2) $(NH_4)_{10}W_{12}O_{41}\cdot 5H_2O$, (3) recovered amorphous ZrW_2O_8, (4) $Na_2WO_4\cdot 2H_2O$ (5) cubic ZrW_2O_8 with those from a ZrW_2O_8 sample at different pressures in a DAC. The vertical line serves as a guide to the eye.

D. *Ex situ* EXAFS

In analyzing the EXAFS data collected for our set of reference compounds and the amorphous ZrW_2O_8 recovered from high pressure, several different models were used. The models and the results from the fits are available as supplementary material.[108] For all of the samples two very simple models consisting of a single W—O path with a multiplicity of 4 and 6 were explored, even though for samples with irregular coordination the fits are inevitably quite poor. This approach was adopted as, in general, the average M-O bond length for a coordination polyhedron increases as the coordination number of the metal increases and this variation is big enough for us to use the refined W—O distance from our EXAFS analyses as an indicator of the coordination number for the tungsten. The average M-O distance has been used as a metric by other workers looking for changes in coordination under pressure.[68,103] In Table I, we present the average W—O bond lengths from our fits; a clear relationship between the average W—O bond length and the coordination number is observed. This relationship can also be seen by a visual inspection of the Fourier-filtered EXAFS data (see Fig. 5). The three compounds with tetrahedral coordination gave average distances of 1.77 Å, but ammonium paratungstate, containing tungsten with heavily distorted octahedral coordination, gave a value of 1.83 Å, WO_3, which also has distorted octahedral coordination, gave a value of 1.83 Å, and Ba_2NiWO_6, which is believed to contain tungsten in a regular octahedral environment,[104] gave a distance of 1.87 Å. The difference between the values for the paratungstate and the perovksite are to be expected, as EXAFS analyses do not give a simple average of the W—O distances around the tungsten because the fits are more sensitive to the short W—O distances in a coordination polyhedron. The average W—O distance obtained from the single pathlength fits to the amorphous ZrW_2O_8 sample, ~1.81 Å, is much shorter than that seen for the reference compound Ba_2NiWO_6, effectively ruling out anything approaching regular octahedral coordination for tungsten in the amorphous sample. However, it is close to, but slightly smaller than, the value obtained for the paratungstate, suggesting that tungsten could have, on average, very irregular six coordination or perhaps five coordination. This interpretation is consistent with that for the XANES data. We performed fits to the data for amorphous zirconium tungstate using models derived from cubic ZrW_2O_8 (1+3 coordination) and orthorhombic ZrW_2O_8 (irregular five coordination). The 1+3 model offered no improvement over the single-path model, but the five-coordinate model gave better fits, again supporting an irregular average coordination environment for the tungsten. However, the XANES data are not consistent with this sample having local environments identical to those in orthorhombic ZrW_2O_8, as our *in situ* XANES measurements indicate that the orthorhombic phase gives a pre-edge feature that is well resolved from the absorption edge.

E. *In situ* EXAFS

In Fig. 2, we show $\chi(k)$ as a function of pressure for ZrW_2O_8 as it is compressed in the DAC along with $\chi(k)$ for cubic ZrW_2O_8 and amorphous ZrW_2O_8 recovered from high pressure. The EXAFS evolve in an apparently continuous fashion from something resembling the starting cubic ZrW_2O_8 at low pressure through to a curve at 7.6 GPa that, at low k, looks very similar to that for the material recovered from high pressure. Qualitatively the low-k EXAFS for the sample at 3.6 GPa (showing only weak, very broad scattering maxima by diffraction) are clearly different from those of the 2.3 GPa sample (orthorhombic by diffraction), indicating a significant change in the local structure between these pressures.

Although the *in situ* EXAFS data are noisy and the $\chi(k)$ at 3.6 and 7.6 GPa are incomplete, we performed a fit to these data using a single W—O path model so that we could look for changes in the average W—O bond length as a function of pressure that are indicative of changes in coordination environment. The details from these fits are available as supplementary material,[108] but the W—O distances are summarized in Table I and the Fourier filtered EXAFS are shown in Fig. 5. There is no apparent change in average W—O distance on going to 0.7 GPa, perhaps because the coordination changes that occur on going from the cubic to the orthorhombic phase primarily involve the introduction of long W—O contacts that do not contribute strongly to the EXAFS average W—O value. On compression to 2.3 GPa, where the sample is still orthorhombic by diffraction, the average W—O distance increases slightly, suggesting that some of the longer W—O contacts are shortening, and in response the shorter W—O contacts are getting longer; effectively the coordination polyhedron is becoming less irregular and hence more compact. At 3.6 GPa, where the sample shows signs of severe structural disorder by diffraction, the average W—O distance increases to a value close to that seen in the sample recovered from 7.5 GPa, again suggesting a further increase in coordination number or regularization of the coordination polyhedra, so that some of the longer contacts that contributed weakly to the average W—O distance contribute more strongly. The average W—O distance from the fit to the data for 7.6 GPa is ~1.86 Å, close to the value seen for octahedral tungsten in Ba_2NiWO_6. However, the 7.6 GPa data are poor enough that this value is questionable.

IV. CONCLUSIONS

Our *in situ* measurements show the expected formation of orthorhombic ZrW_2O_8 at low pressure followed by the onset of amorphization above 2.3 GPa with completion by ~7.6 GPa. The XAS data support a continuous evolution of the local tungsten coordination environment on compression after forming the orthorhombic phase, with the average W—O bond length increasing, indicating an increase in the average coordination number, and the W L_I pre-edge peak decreasing in magnitude, indicating a movement toward tungsten coordination that is closer to centrosymmetric. While the 7.6 GPa XAS data is consistent with the presence of some tungsten with octahedral coordination, the data is of insufficient quality to be sure of this. On the basis of a high-pressure simulation study,[62] it has been suggested that changes in zirconium coordination as pressure increases are more likely than changes in the tungsten coordination. Our observation of large changes in tungsten coordination under pressure are either inconsistent with this study or indicate that there must be large changes in zirconium coordination as well. The *in situ* XANES measurements on ZrW_2O_8 clearly differ from the *ex situ* measurements made on an amorphous sample recovered from 7.6 GPa in a multianvil press. These XANES suggest a structural relaxation of a glass that initially contains almost octahedral tungsten to a material containing tungsten in heavily distorted octahedral coordination similar to that found in ammonium paratungstate.

Our measurements are not consistent with a mechanism for amorphization that primarily involves reorienting existing coordination polyhedra in a disordered fashion. From the perspective of tungsten coordination, the *in situ* data are consistent with initial transformation to the orthorhombic phase, containing 4-, 4+1-, and 4+2-coordinated tungsten, followed by a shortening of the long W—O contacts that exist in this structure, as the sample is further compressed. This regularization of the coordination environments seems to continue into the pressure regime where the sample becomes amorphous.

Measurements showing changes in longer range local structure (M—M distances) and the zirconium coordination environment would be helpful in providing a better picture of the amorphization process. Ideally these should be made *in situ*, as our current data suggest that structural relaxation on decompression is a problem.

ACKNOWLEDGMENTS

This work is based upon research conducted at the Cornell High Energy Synchrotron Source (CHESS), which is supported by the National Science Foundation and the National Institutes of Health/National Institute of General Medical Sciences under Award DMR-0225180. We are grateful to the staff of CHESS, particularly K. Finkelstein, for help and guidance. We acknowledge the Mineral Physics Institute of SUNY Stony Brook for providing access to the high pressure apparatus and technical support. APW is grateful for support under National Science Foundation Grant No. DMR-0203342.

[1] O. Mishima, L. D. Calvert, and E. Whalley, Nature (London) **310**, 393 (1984).
[2] R. J. Hemley, A. P. Jephcoat, H.-K. Mao, L. C. Ming, and M. H. Manghnani, Nature (London) **334**, 52 (1988).
[3] M. B. Kruger and R. Jeanloz, Science **249**, 647 (1990).
[4] E. G. Ponyatovsky and O. I. Barkalov, Mater. Sci. Rep. **8**, 147 (1992).
[5] A. Jayaraman, S. K. Sharma, Z. Wang, S. Y. Wang, L. C. Ming, and M. H. Manghnani, J. Phys. Chem. Solids **54**, 827 (1993).
[6] S. M. Sharma and S. K. Sikka, Prog. Mater. Sci. **40**, 1 (1996).
[7] P. Richet and P. Gillet, Eur. J. Mineral. **9**, 907 (1997).
[8] J. Badro, P. Gillet, and J.-L. Barrat, Europhys. Lett. **42**, 643 (1998).
[9] T. Sakuntala, A. K. Arora, N. V. Chandra Shekar, and P. C. Sahu, J. Clin. Eng. **12**, 4417 (2000).
[10] V. Dmitriev, V. Sinitsyn, R. Dilanian, D. Machon, A. Kuznetsov, E. Ponyatovsky, G. Lucazeau, and H. P. Weber, J. Phys. Chem. Solids **64**, 307 (2003).
[11] H. Liu, R. A. Secco, N. Imanaka, and G. Adachi, Solid State Commun. **121**, 177 (2002).
[12] A. Grzechnik and W. A. Crichton, Solid State Sci. **4**, 1137 (2002).
[13] C. Lind, D. G. VanDerveer, A. P. Wilkinson, J. Chen, M. T. Vaughan, and D. J. Weidner, Chem. Mater. **13**, 487 (2001).
[14] C. A. Perottoni and J. A. H. de Jornada, Science **280**, 886 (1998).
[15] R. A. Secco, H. Liu, N. Imanaka, and G. Adachi, J. Mater. Sci. Lett. **20**, 1339 (2001).
[16] R. J. Speedy, J. Clin. Eng. **8**, 10907 (1996).
[17] A. W. Sleight, Inorg. Chem. **37**, 2854 (1998).
[18] A. W. Sleight, Annu. Rev. Mater. Sci. **28**, 29 (1998).
[19] A. W. Sleight, Curr. Opin. Solid State Mater. Sci. **3**, 128 (1998).
[20] J. S. O. Evans, J. Chem. Soc. Dalton Trans. **1999**, 3317.
[21] R. Mittal, S. L. Chaplot, A. I. Kolesnikov, C.-K. Loong, and T. A. Mary, Phys. Rev. B **68**, 054302 (2003).
[22] R. Mittal, S. L. Chaplot, H. Schober, and T. A. Mary, Phys. Rev. Lett. **86**, 4692 (2001).
[23] R. Mittal, S. L. Chaplot, H. Schober, A. I. Kolesnikov, C.-K. Loong, C. Lind, and A. P. Wilkinson, Phys. Rev. B **70**, 214303 (2004).
[24] T. R. Ravindran, A. K. Arora, and T. A. Mary, Phys. Rev. Lett. **84**, 3879 (2000).
[25] T. R. Ravindran, A. K. Arora, and T. A. Mary, J. Phys.: Condens. Matter **13**, 11573 (2001).
[26] B. Chen, D. V. S. Muthu, Z. X. Liu, A. W. Sleight, and M. B. Kruger, Phys. Rev. B **64**, 214111 (2001).
[27] Y. Yamamura, N. Nakajima, T. Tsuji, M. Koyano, Y. Iwasa, S. Katayama, K. Saito, and M. Sorai, Phys. Rev. B **66**, 014301 (2002).
[28] J. S. O. Evans, Z. Hu, J. D. Jorgensen, D. N. Argyriou, S. Short, and A. W. Sleight, Science **275**, 61 (1997).
[29] Z. Hu, J. D. Jorgensen, S. Teslic, S. Short, D. N. Argyriou, J. S. O. Evans, and A. W. Sleight, Physica B **241–243**, 370 (1998).
[30] J. D. Jorgensen, Z. Hu, S. Teslic, D. N. Argyriou, S. Short, J. S. O. Evans, and A. W. Sleight, Phys. Rev. B **59**, 215 (1999).
[31] J. M. Gallardo-Amores, U. Amador, E. Moran, and M. A. Alario-Franco, Int. J. Inorg. Mater. **2**, 123 (2000).
[32] J. D. Jorgensen, Z. Hu, S. Short, A. W. Sleight, and J. S. O. Evans, J. Appl. Phys. **89**, 3184 (2001).
[33] S. Carlson and A. M. Krogh Andersen, J. Appl. Crystallogr. **34**, 7 (2000).
[34] T. Varga, A. P. Wilkinson, C. Lind, W. A. Bassett, and C.-S. Zha, Phys. Rev. B **71**, 214106 (2005).
[35] W. Paraguassu, M. Maczka, A. G. Souza Filho, P. T. C. Freire, J. Mendes Filho, F. E. A. Melo, L. Macalik, L. Gerward, J. Staun Olsen, A. Waskowska, and J. Hanuza, Phys. Rev. B **69**, 094111 (2004).
[36] M. Maczka, W. Paraguassu, A. G. Souza Filho, P. T. C. Freire, J. Mendes Filho, F. E. A. Melo, and J. Hanuza, J. Comput. Chem. **177**, 2002 (2004).
[37] G. D. Mukherjee, S. N. Achary, A. K. Tyagi, and S. N. Vaidya, J. Phys. Chem. Solids **64**, 611 (2003).
[38] A. K. Arora, R. Nithya, T. Yagi, N. Miyajima, and T. A. Mary, Solid State Commun. **129**, 9 (2004).
[39] J. S. O. Evans, T. A. Mary, and A. W. Sleight, J. Solid State Chem. **133**, 580 (1997).
[40] J. S. O. Evans and T. A. Mary, Int. J. Inorg. Mater. **2**, 143 (2000).
[41] A. K. Tyagi, S. N. Achary, and M. D. Mathews, J. Alloys Compd. **339**, 207 (2002).
[42] D. K. Balch and D. C. Dunand, Metall. Mater. Trans. A **35A**, 1159 (2004).
[43] H. Holzer and D. C. Dunand, J. Mater. Res. **14**, 780 (1999).
[44] C. Verdon and D. C. Dunand, Scr. Mater. **36**, 1075 (1997).
[45] T. A. Mary, J. S. O. Evans, T. Vogt, and A. W. Sleight, Science **272**, 90 (1996).
[46] J. S. O. Evans, T. A. Mary, T. Vogt, M. A. Subramanian, and A. W. Sleight, Chem. Mater. **8**, 2809 (1996).
[47] M. Auray and M. Quarton, Acta Crystallogr., Sect. C: Cryst. Struct. Commun. **51**, 2210 (1995).
[48] N. Duan, U. Kamerwari, and A. W. Sleight, J. Am. Chem. Soc. **121**, 10432 (1999).
[49] J. S. O. Evans, W. I. F. David, and A. W. Sleight, Acta Crystallogr., Sect. B: Struct. Sci. **55**, 333 (1999).
[50] K. Wang and R. R. Reeber, Appl. Phys. Lett. **76**, 2203 (2000).
[51] Y. Yamamura, N. Nakajima, T. Tsuji, Y. Iwasa, K. Saito, and M. Sorai, Solid State Commun. **121**, 213 (2002).
[52] R. Stevens, J. Linford, B. F. Woodfield, J. Boerio-Goates, C. Lind, A. P. Wilkinson, and G. Kowach, J. Chem. Thermodyn. **35**, 919 (2003).
[53] W. I. F. David, J. S. O. Evans, and A. W. Sleight, Europhys. Lett. **46**, 661 (1999).
[54] A. Grzechnik, W. A. Crichton, K. Syassen, P. Adler, and M. Mezouar, Chem. Mater. **13**, 4255 (2001).
[55] D. A. Fleming, D. W. Johnson, and P. J. Lemaire, U.S. Patent 5,694,503, Lucent Technologies, USA, 1997.
[56] D. A. Fleming, P. J. Lemaire, and D. W. Johnson, European Patent EP 97-306798 19970902, Lucent Technologies, Inc., USA, 1998.
[57] D. Cao, F. Bridges, G. R. Kowach, and A. P. Ramirez, Phys. Rev. Lett. **89**, 215902 (2002).
[58] D. Cao, F. Bridges, G. R. Kowach, and A. P. Ramirez, Phys. Rev. B **68**, 014303 (2003).
[59] G. Ernst, C. Broholm, G. R. Kowach, and A. P. Ramirez, Nature (London) **396**, 147 (1998).
[60] A. P. Ramirez and G. R. Kowach, Phys. Rev. Lett. **80**, 4903 (1998).
[61] A. K. A. Pryde, K. D. Hammonds, M. T. Dove, V. Heine, J. D. Gale, and M. C. Warren, Phase Transitions **61**, 141 (1997).
[62] A. K. A. Pryde, M. T. Dove, and V. Heine, J. Clin. Eng. **10**, 8417 (1998).
[63] T. Yamanaka, T. Nagai, and T. Tsuchiya, Z. Kristallogr. **212**, 401

(1997).
[64] A. K. Arora, Solid State Commun. **115**, 665 (2000).
[65] A. S. Pereira, C. A. Perottoni, and J. A. H. Jornada, J. Raman Spectrosc. **34**, 578 (2003).
[66] R. J. Hemley, C. Meade, and H. K. Mao, Phys. Rev. Lett. **79**, 1420 (1997).
[67] M. Guthrie, C. A. Tulk, C. J. Benmore, J. Xu, J. L. Yarger, D. D. Klug, J. S. Tse, H. K. Mao, and R. J. Hemley, Phys. Rev. Lett. **93**, 115502 (2004).
[68] C. Meade, R. J. Hemley, and H. K. Mao, Phys. Rev. Lett. **69**, 1387 (1992).
[69] G. Shen, V. B. Prakapenka, M. L. Rivers, and S. R. Sutton, Rev. Sci. Instrum. **74**, 3021 (2003).
[70] A. V. Sapelkin and S. C. Bayliss, High Press. Res. **21**, 315 (2001).
[71] R. Ingalls, G. A. Garcia, and E. A. Stern, Phys. Rev. Lett. **40**, 334 (1978).
[72] R. Ingalls, E. D. Crozier, J. E. Whitmore, A. J. Seary, and J. M. Tranquada, J. Appl. Phys. **51**, 3158 (1980).
[73] K. Ohsumi, S. Sueno, I. Nakai, M. Imafuku, H. Morikawa, M. Kimata, M. Nomura, and O. Shimomura, J. Phys. (Paris) **47**, 189 (1986).
[74] S. Sueno, I. Nakai, M. Imafuku, H. Morikawa, M. Kimata, K. Ohsumi, M. Nomura, and O. Shimomura, Chem. Lett. **10**, 1663 (1986).
[75] H. Tolentino, E. Dartyge, A. Fontaine, and G. Tourillon, J. Appl. Crystallogr. **21**, 15 (1988).
[76] S. Pascarelli, O. Mathon, and G. Aquilanti, J. Alloys Compd. **362**, 33 (2004).
[77] S. H. Tolbert and A. P. Alivisatos, NATO ASI Ser., Ser. E **260**, 471 (1994).
[78] Z. Hu, S. Bertram, and G. Kaindl, Phys. Rev. B **49**, 39 (1994).
[79] G. Kaindl, G. Schmiester, E. V. Sampathkumaran, and P. Wachter, Phys. Rev. B **38**, R10174 (1988).
[80] A. Yoshiasa, T. Nagai, O. Ohtaka, O. Kamishima, and O. Shimomura, J. Synchrotron Radiat. **6**, 43 (1999).
[81] W. A. Bassett, A. J. Anderson, R. A. Mayanovic, and I.-M. Chou, Chem. Geol. **167**, 3 (2000).
[82] W. A. Bassett, A. H. Shen, M. Bucknum, and I.-M. Chou, Rev. Sci. Instrum. **64**, 2340 (1993).
[83] K. Largarec and S. Desgreniers, computer code Simplified Image Plate Analysis, University of Ottawa, Ottawa, ON, Canada (1994–1997).
[84] JADE, computer code for XRD Pattern Processing, Materials Data, Inc., Livermore, CA (1995–2005).
[85] A. C. Larson and R. B. Von Dreele, computer code General Structural Analysis System, Los Alamos National Laboratory, Los Alamos, NM, 2000.
[86] J. Zhao, computer code Calibration, University of Witwatersrand, Johannesburg-Gauteng, South Africa, 1998.
[87] F. Birch, J. Geophys. Res. B **91**, 4949 (1986).
[88] B. Ravel, computer code ATHENA, Naval Research Laboratory, Washington, DC, 2005.
[89] M. Newville, J. Synchrotron Radiat. **8**, 322 (2001).
[90] L. Dubrovinsky, N. Dubrovinskaia, S. Saxena, and T. LiBehan, Mater. Sci. Eng., A **A288**, 187 (2000).
[91] N. Funamori, M. Funamori, R. Jeanloz, and N. Hamaya, J. Appl. Phys. **82**, 142 (1997).
[92] H. Libotte and J.-P. Gaspard, Phys. Rev. B **62**, 7110 (2000).
[93] T. Taniguchi, T. Sato, W. Utsumi, T. Kikegawa, and O. Shimomura, Appl. Phys. Lett. **70**, 2392 (1997).
[94] T.-C. Wu, W. A. Bassett, P. C. Burnley, and M. S. Weathers, J. Geophys. Res. **98**, 19767 (1993).
[95] J. Wong, F. W. Lytle, R. P. Messmer, and D. H. Maylotte, Phys. Rev. B **30**, 5596 (1984).
[96] A. Balerna, E. Bernieri, E. Burattini, A. Kuzmin, A. Lusis, J. Purans, and P. Cikmach, Nucl. Instrum. Methods Phys. Res. A **308**, 234 (1991).
[97] J. A. Horsley, I. E. Wachs, J. M. Brown, G. H. Via, and F. D. Hardcastle, J. Phys. Chem. **91**, 4014 (1987).
[98] F. Hilbrig, H. E. Gobel, H. Knozinger, H. Schmelz, and B. Lengeler, J. Phys. Chem. **95**, 6973 (1991).
[99] v. H. D'Amour and R. Allman, Z. Kristallogr. **136**, 23 (1972).
[100] Y. N. Xu, S. Carlson, and R. Norrestam, J. Solid State Chem. **132**, 123 (1997).
[101] V. S. Filip'ev, G. E. Shatalova, and E. G. Fesenko, Kristallografiya **19**, 386 (1974).
[102] D. L. Decker, J. Appl. Phys. **42**, 3239 (1971).
[103] J. P. Itie, A. Polian, G. Calas, J. Petiau, A. Fontaine, and H. Tolentino, Phys. Rev. Lett. **63**, 398 (1989).
[104] D. E. Cox, G. Shirane, and B. C. Frazer, J. Appl. Phys. **38**, 1459 (1967).
[105] J. S. O. Evans, T. A. Mary, and A. W. Sleight, J. Solid State Chem. **137**, 148 (1998).
[106] K. Okada, H. Morikawa, F. Marumo, and S.-i. Iwai, Bull. Tokyo Inst. Technol. **120**, 7 (1974).
[107] P. M. Woodward, A. W. Sleight, and T. Vogt, J. Phys. Chem. Solids **56**, 1305 (1995).
[108] See EPAPS Document No. E-PRBMDO-72-024526 for supplementary material containing details of the EXAFS fits. For more information on EPAPS, see http://www.aip.org/pubservs/epaps.html.